PALEOCLIMATE

Biogeographic climate sensitivity controls Earth system response to large igneous province carbon degassing

Julian Rogger[1,2]*, Emily J. Judd[3], Benjamin J. W. Mills[4], Yves Goddéris[5], Taras V. Gerya[1], Loïc Pellissier[2,6]

Periods of large igneous province (LIP) magmatism have shaped Earth's biological and climatic history, causing major climatic shifts and biological reorganizations. The vegetation response to LIP-induced perturbations may affect the efficiency of the carbon-climate regulation system and the post-LIP climate evolution. Using an eco-evolutionary vegetation model, we demonstrate here that the vegetation's climate adaptation capacity, through biological evolution and geographic dispersal, is a major determinant of the severity and longevity of LIP-induced hyperthermals and can promote the emergence of a new climatic steady state. Proxy-based temperature reconstructions of the Permian-Triassic, Triassic-Jurassic, and Paleocene-Eocene hyperthermals match the modeled trajectories of bioclimatic disturbance and recovery. We conclude that biological vegetation dynamics shape the multimillion-year Earth system response to sudden carbon degassing and global warming episodes.

Large igneous provinces (LIPs) represent major perturbations to the Earth system, triggering environmental changes that can result in severe mass extinctions on land and in the ocean (*1*, *2*). Climate warming after the degassing of massive amounts of carbon in geologically instantaneous time is considered one of the main triggers of LIP-associated biological extinctions and reorganizations (*1*). The severity and duration of the climate perturbation depend on how fast the emitted carbon is returned to Earth's interior by climate feedback mechanisms such as silicate mineral weathering and organic carbon burial (*3*, *4*). The efficiency of the carbon-climate regulation system, however, may in turn be affected by terrestrial and marine ecosystems being shifted to a state of disequilibrium and maladaptation (*5*–*8*).

The terrestrial vegetation plays an integral part in the long-term carbon-climate regulation system, but its functioning is sensitive to abrupt environmental changes. Primary productivity determines the extent of photosynthetic carbon assimilation and the burial of organic carbon as a net CO_2 sink. Vegetation can further enhance CO_2 consumption through silicate mineral–weathering reactions, for example, by releasing reactive species such as organic acids and chelators into the soil during nutrient acquisition or by intensifying the local hydrological cycle and prolonging water-mineral contact times (*9*–*14*). LIP-triggered environmental perturbations modify vegetation structure and functioning, causing species extinctions, range shifts, deforestation, reductions in organic carbon burial, and the spread of opportunistic species into newly freed habitats until more adapted plant communities reestablish (*5*–*7*, *15*–*17*). To what extent and how fast vegetation functions recover from LIP-induced climatic changes depends on the capacity of plants to disperse and follow suitable habitats in a given paleogeographic setting (*18*) and to adjust to new conditions through evolutionary adaptation (*19*, *20*). After the most severe mass extinction in Earth's history around 252 million years (Ma) ago, which was triggered by the Siberian Traps LIP, the recovery of vegetation diversity and productivity to pre-LIP levels required several million years (*7*, *15*, *16*). During this recovery period, the efficiency of the carbon-climate regulation system may have been reduced due to weakened vegetation-weathering interactions and reduced primary productivity. The long-term climatic consequences of LIP degassing events may be dictated not only by intrinsic characteristics of the LIP episode, such as the mass of emitted greenhouse gases, but also by the biological response and bioclimatic interactions in a given paleogeographic setting.

Here, we used an eco-evolutionary vegetation model and proxy-based temperature reconstructions to investigate how the climate adaptation capacity of vegetation, by dispersal and adaptive evolution, may have affected geologic carbon fluxes and long-term climate evolution after episodes of Phanerozoic LIP degassing. We consider three LIPs, the Siberian Traps (Permian-Triassic boundary, ≈252 Ma), the Central Atlantic Magmatic Province (Triassic-Jurassic boundary, ≈ 201 Ma), and the North Atlantic Igneous Province (Paleocene-Eocene boundary, ≈56 Ma). The LIPs differed in the severity of the triggered biological and climatic consequences and occurred under contrasting paleogeographic configurations. During the Siberian Traps and the Central Atlantic Magmatic Province, most continental land mass was assembled in the supercontinent Pangea. The two LIPs are assumed to have caused two of the most severe mass extinctions in Earth's history (*1*). The Siberian Traps further resulted in a multimillion-year hyperthermal of elevated atmospheric CO_2 and temperatures (*21*, *22*). The North Atlantic Igneous Province occurred under a more modern paleogeography with dispersed continents, and it caused the most severe warming event during the Cenozoic, the Paleocene-Eocene Thermal Maximum (PETM) (*23*). Although less severe in terms of species extinctions, the PETM still induced a major reorganization of biological systems on land and in the ocean (*24*).

Our eco-evolutionary model is designed to capture major vegetation dynamics in response to climate perturbations, including dispersal, adaptation, and competition, and is coupled to models of the geologic carbon cycle and climate. The climate trajectory after an imposed LIP degassing episode depends on how fast the released carbon is returned from the atmosphere-ocean system to geologic carbon reservoirs through silicate weathering and organic carbon burial. Silicate weathering is modeled as a function of local erosion, runoff, temperature, and vegetation-mediated weathering enhancement. In areas of high plant productivity, a maximum fourfold or sixfold (see the supplementary materials) weathering enhancement is considered compared with unvegetated land (*9*, *10*, *12*, *25*). Marine organic carbon production and burial depend on local sea surface temperatures and continental weathering as a nutrient source, whereas vegetation productivity and terrestrially derived organic carbon burial depend on solar radiation, aridity, temperature, and the vegetation adaptation state. Primary productivity and weathering enhancement are calculated by modeling vegetation units that populate the continents and that can disperse and adapt in response to climatic changes at specified rates. The vegetation units represent plant assemblages, which we call "floras," and depict the ensemble response of their constituents. Floras are characterized by a Gaussian niche, defined by an optimum mean annual temperature (MAT) and the Budyko aridity index (BAI) at which their physiological potential is greatest. The climate niche determines a geographic space in which a flora can be productive (niche range of 10°C in MAT and two BAI units; see the supplementary materials and fig. S1 for derivation). The LIP-triggered climate warming can cause a discrepancy between a flora's optimum niche and the local environment, resulting in reduced productivity

[1]Department of Earth Sciences, ETH Zurich, Zurich, Switzerland. [2]Department of Environmental Systems Science, ETH Zurich, Zurich, Switzerland. [3]Department of Geosciences, University of Arizona, Tucson, Arizona, USA. [4]School of Earth and Environment, University of Leeds, Leeds, UK. [5]Géosciences-Environnement Toulouse, CNRS-Observatoire Midi-Pyrénées, Toulouse, France. [6]Swiss Federal Institute for Forest, Snow and Landscape Research, Birmensdorf, Switzerland.
*Corresponding author. Email: julian.rogger@erdw.ethz.ch

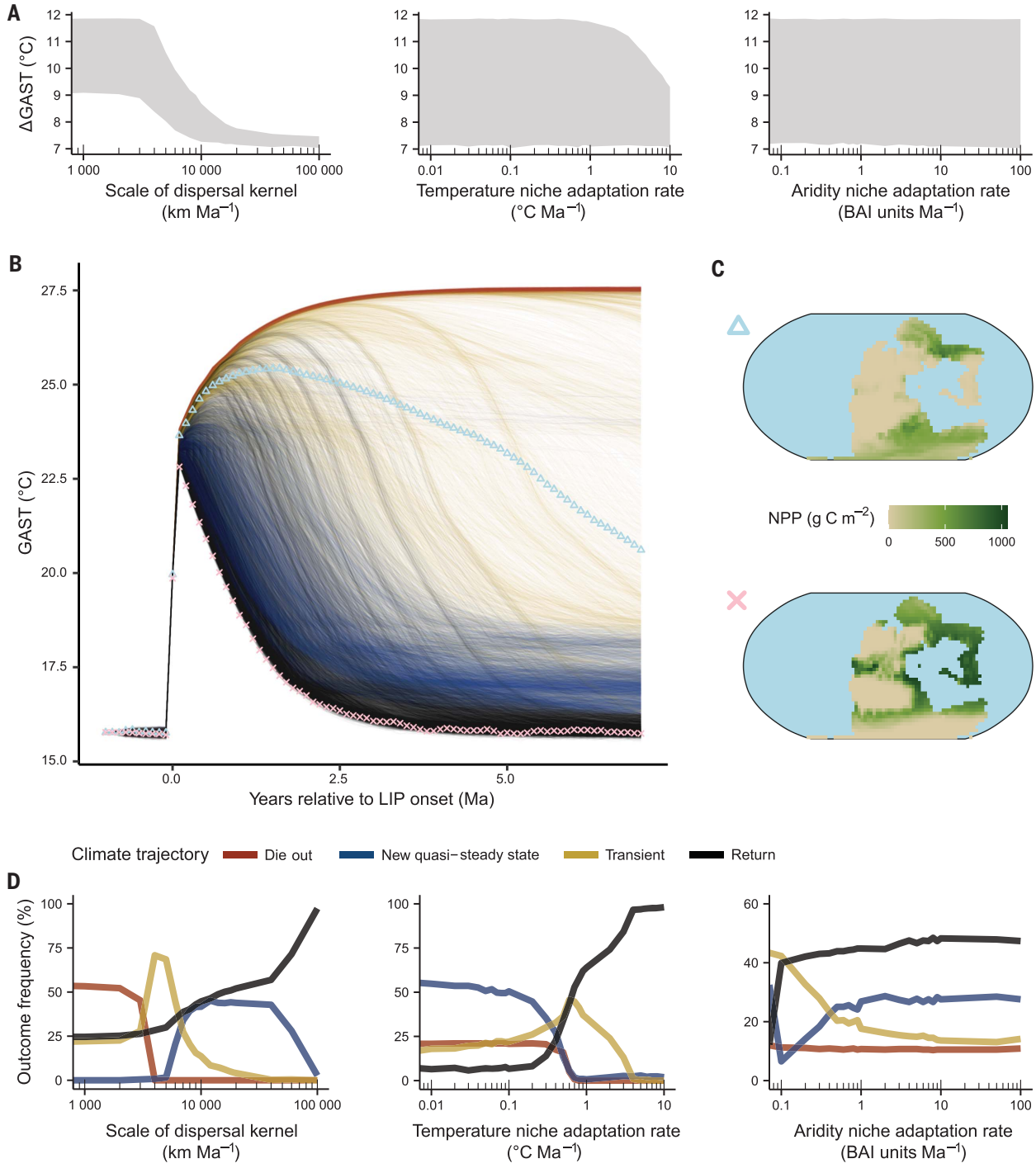

Fig. 1. Sensitivity of modeled post-LIP climate trajectories to eco-evolutionary vegetation dynamics. (**A**) The range of modeled GAST warming depending on the vegetation's adaptation capacity. The dispersal value represents the scale parameter of a Weibull distribution with shape parameter value of two, from which dispersal values of modeled floras are randomly drawn. A flora's aridity niche is characterized by a range of the BAI. The aridity adaptation rate is thus expressed as BAI units per million years. (**B**) The climate trajectories observed for different vegetation adaptation capacities. Each line represents a separate model run with a different combination of vegetation dispersal capacity and climate niche adaptation rates. The die-out trajectories include outcomes with $<10^{12}$ mol C year^{-1} terrestrial organic carbon burial at the end of the simulation and a high-temperature steady state. The return trajectories indicate a complete recovery of climate from the perturbation (ΔGAST between the end and beginning of the simulation <0.5°C). The new quasi–steady-state trajectories represent a stabilization of climate at a higher GAST (minimum of +0.5°C compared with initial conditions, ΔGAST <0.5°C and change in terrestrial organic carbon burial $<5 \times 10^{10}$ mol C year^{-1} during the last two million model years). In the transient trajectories none of the above occurs until the end of the simulation. All carbon fluxes associated with the different climate trajectories are shown in fig. S2. (**C**) Spatial net primary productivity (NPP) plots showing the distribution of productivity for a return (bottom) and a transient (top) trajectory 2 Ma after the LIP onset. (**D**) Model outcome frequency depending on biological adaptation parameters. In total, 12,122 parameter combinations were tested (19 Weibull dispersal scale parameters and 29 temperature- and 22 aridity-adaptation rates).

and vegetation-mediated weathering enhancement until a better-adapted flora disperses to the location or the original flora adapts to the new conditions through adaptive evolution. By testing a wide parameter range for rates of flora dispersal (varying the scale parameter of the dispersal kernel between 0 and 100,000 km Ma^{-1}) and niche evolution (varying the rates of temperature niche adaptation from 0 to 10°C Ma^{-1} and aridity niche adaptation from 0 to 100 BAI units Ma^{-1}), we explored the sensitivity of LIP-triggered climatic perturbations to the vegetation's adaptation capacity in a given paleogeographic configuration.

Vegetation recovery shapes long-term climate trajectory and steady state

The vegetation's climate adaptation capacity and its effects on organic carbon burial and silicate-weathering rates affect the severity and duration of the temperature excursion, as well as the long-term climatic steady state, after a LIP degassing event (Fig. 1A). Using the paleogeography of the Permian-Triassic mass extinction and a LIP degassing of 40,000 Gt of carbon in 200,000 years (*3*), the modeled global average surface temperature (GAST) warming is between 7° and 12°C, with greater warming in simulations in which floras have a limited capacity to disperse in geographic space or to adapt their climatic niche to local environmental conditions by adaptive evolution. The climate trajectories recovered from the simulations show four categories of behavior (Fig. 1B): the "return," "die-out," "new quasi–steady-state," and "transient" trajectories. Return trajectories describe a full recovery of the GAST to temperatures similar to those before the degassing event. This scenario is characterized by an ephemeral temperature excursion during which carbon sinks temporarily fail to effectively remove carbon from the atmosphere-ocean system. This is caused by a vegetation adaptation lag, resulting in reductions in vegetation-mediated weathering enhancement and organic carbon burial. During the temperature excursion, these processes can temporarily offset the effects of higher temperatures and a more active hydrological cycle on silicate weathering. As the vegetation recovers, the strength of carbon-feedback mechanisms is reestablished, and excess carbon is effectively removed from the atmosphere-ocean system (a complete set of carbon fluxes is shown in fig. S2).

In a large proportion of the simulations, a new quasi–steady-state climate emerges, which is characterized by stabilization of the GAST at a higher temperature than before the degassing event. This scenario is characterized by carbon flux dynamics similar to those in the return scenario, with the exception that the vegetation does not fully recover from the climatic perturbation. As a result, land-derived organic carbon burial and vegetation-mediated silicate-weathering enhancement stabilize at a lower level than before the degassing event, resulting in a higher GAST. The new quasi–steady-state temperature is high enough that the direct climatic effects of temperature and increased runoff on silicate weathering counterbalance the solid Earth carbon degassing despite the less adapted vegetation. A full vegetation recovery is prevented by the presence of dispersal barriers (e.g., oceans, deserts, and areas with better-adapted competitors) that hinder floras in following their optimum climatic niche under a limited speed of in situ evolutionary adaptation. The resulting climate state is considered a quasi–steady state because continued adaptive evolution, changes in degassing rates, or paleogeography beyond the considered model duration would promote further climatic changes.

The transient category includes climate trajectories that reached neither the initial nor a new quasi–steady-state GAST within the modeled period but would presumably do so if a longer time horizon was considered. Finally, die-out trajectories correspond to situations in which the terrestrial vegetation is not able to cope with the climatic changes and possibly vanishes completely. In this trajectory, temperatures continue to increase until silicate weathering can compensate for the carbon degassing in the absence of vegetation.

The trajectory of a LIP-triggered carbon-climate excursion is determined by the combination of the vegetation's dispersal and climate adaptation capacity (Fig. 1D). Die-out trajectories are limited to models assuming very low dispersal capacities. For temperature adaptation rates lower than 1°C Ma^{-1}, simulations predict an increased likelihood of reaching a new climatic quasi–steady state. This is because the warming exceeds the in situ temperature adaptation capacity, thus triggering a dispersal response and a redistribution of floras, which can result in an incomplete recovery and less-productive vegetation distribution. The aridity adaptation capacity limits the geographic space into which a flora can disperse. Therefore, simulations predict an increased proportion of transient trajectories with a slow climatic recovery in the low-aridity adaptation range. We observed a full recovery from the climate perturbation only in simulations considering the highest dispersal and temperature adaptation rates, enabling floras to efficiently track their climatic niche or eliminate the need for migration, respectively. Such dispersal and temperature niche adaptation rates represent the upper end of what can be considered a plausible range for plants (*18*–*20*, *26*, *27*). Considering more likely temperature niche adaptation rates of 0 to 3°C Ma^{-1} (median <1°C) (*19*, *26*), nonzero aridity adaptation (*19*), and the exclusion of unrealistic dispersal values that result in die-out trajectories, all three of the categories, return, new quasi–steady state, and transient, are plausible climate trajectories after a LIP degassing of the intensity estimated to have occurred at the Permian-Triassic boundary.

Bioclimatic response to Phanerozoic LIPs

Simulations produce climate trajectories that correspond well with the variable temperature responses reconstructed for different Phanerozoic LIPs (Fig. 2). We compiled multimillion-year composite sea surface temperature reconstructions spanning the emplacement and aftermath of the Siberian Traps, the Central Atlantic Igneous Province, and the North Atlantic Igneous Province LIPs based on several geochemical proxy systems and from different locations around the globe (see the supplementary materials). We applied the coupled vegetation–carbon-cycle model to the corresponding paleogeographic settings and varied boundary conditions, i.e., pre-LIP atmospheric CO_2 concentration and mass and duration of the LIP carbon degassing, within estimated ranges [600 ppm, 40,000 Gt C, 200 ka, for the Siberian Traps (*21*, *28*, *29*); 800 ppm, 30,000 Gt C, 200 ka, for the Central Atlantic Igneous Province (*30*, *31*); and 500 ppm, 15,000 Gt C, 100 ka (step injection) (*32*–*34*), for the North Atlantic Igneous Province; alternative scenarios are shown in fig. S3]. In doing so, we identified eco-evolutionary vegetation dynamics as a possible cause of the variability in post-LIP climate evolution, excluding models with unrealistic dispersal scales that would result in die-out trajectories and considering only models with nonzero temperature and aridity niche adaptation rates.

Geologic proxies suggest the most severe and sustained warming for the Siberian Traps (Permian-Triassic), with temperatures increasing by 5° to 10°C over 5 Ma after the LIP and a subsequent recovery of temperatures to about 2.5°C higher than before the LIP. This severity and multimillion-year warming, as well as a possible shift to a new climate quasi–steady state, is reproduced in the model when a strongly affected vegetation with a limited climate adaptation capacity by dispersal and evolution is assumed, resulting in a sustained reduction of the efficiency of the carbon-climate regulation system. The resulting reduction in the ratio of organic to total carbon burial further results in an excursion of approximated carbonate $\delta^{13}C$ signatures, in agreement with proxy records for the period (up to −6‰; fig. S4). Applying the same biological parameter space to the Central Atlantic Igneous Province (Triassic-Jurassic), we simulate less severe temperature excursions, with an initial warming of ~5°C and a relatively rapid and continuous recovery of temperatures thereafter, consistent with the proxy data. This suggests a faster recovery of vegetation and carbon-cycle feedback mechanisms after the LIP perturbation, with the excess carbon being captured effectively through

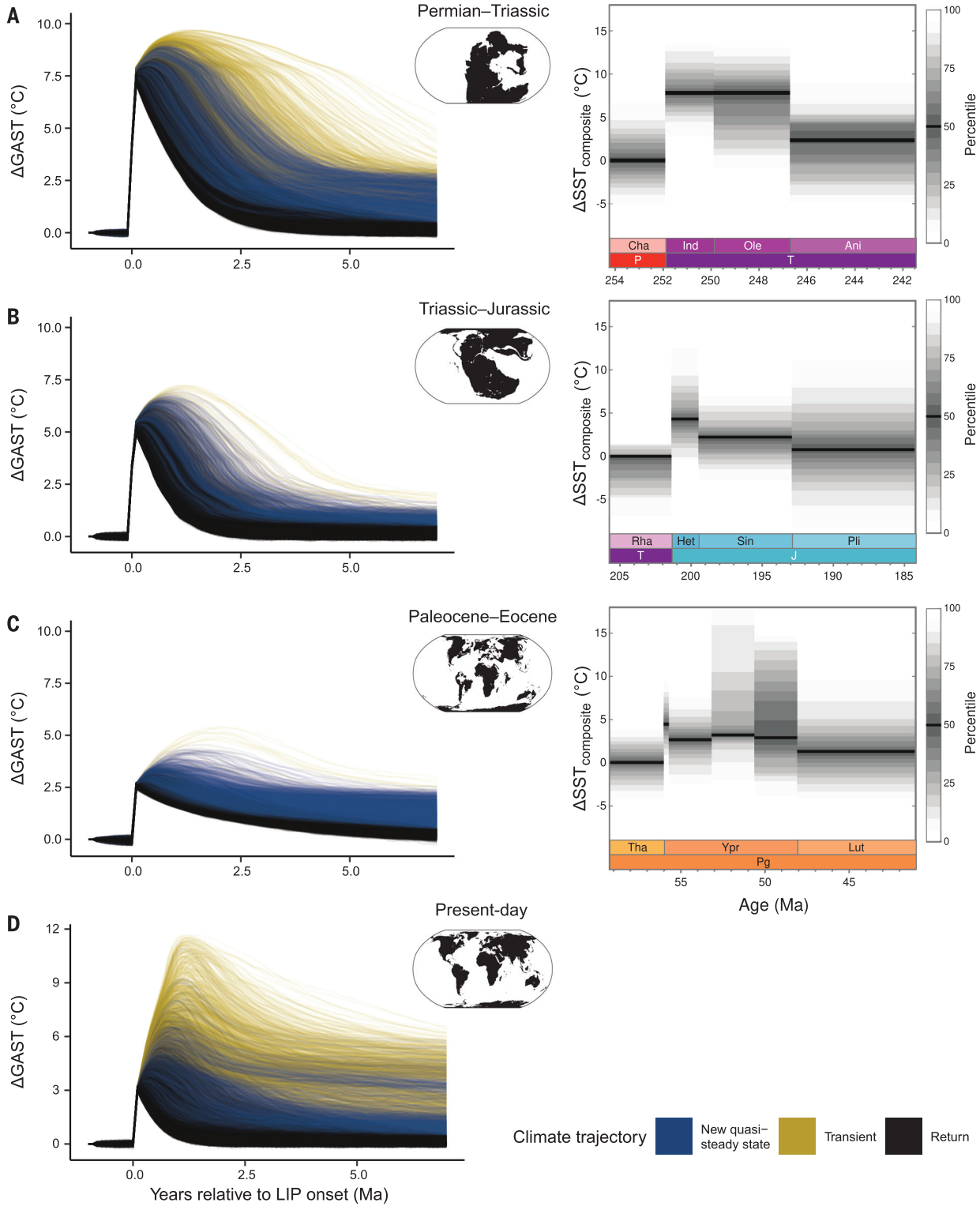

Fig. 2. Comparison of modeled and reconstructed temperature changes for different Phanerozoic LIP degassing events. $\Delta SST_{composite}$ represents a composite sea surface temperature change reconstructed from several geologic proxy systems and sample locations around the globe based on data compiled in the PhanSST database (*53*) (see the supplementary materials for the derivation of temperature values). (**A**) Siberian Traps LIP (Permian-Triassic boundary). (**B**) Central Atlantic Magmatic Province (Triassic-Jurassic boundary). (**C**) North Atlantic Igneous Province (Paleocene-Eocene boundary). (**D**) Hypothetical LIP scenario for present-day geography. For all LIPs, the same parameter range for vegetation dynamics was considered: dispersal scale >5000 km Ma^{-1}, temperature niche adaptation >0°C Ma^{-1}, aridity niche adaptation >0 BAI units Ma^{-1}. See the main text for pre-LIP starting CO_2 concentration, LIP C degassing mass, and LIP duration. An alternative set of scenarios regarding the magnitude and duration of degassing, as well as sensitivity to plant-weathering enhancement, is explored in fig. S3. Paleogeographies are taken from (*56*) and (*57*).

silicate weathering and organic carbon burial. For the North Atlantic Igneous Province, the proxy record reveals a short-lived initial warming of 3 to 5°C (the PETM), followed by a multimillion-year increase in temperatures of ~2.5°C (the Early Eocene Climatic Optimum). This is in agreement with a large range of possible new climatic quasi–steady states modeled for the respective paleogeography. We further modeled a hypothetical LIP of 10,000 Gt C to test the response for the present-day continental configuration, assuming a starting CO_2 concentration of 400 ppm. Despite the lower mass of carbon injected, a similar set of trajectories as for the Permian-Triassic is observed, ranging from rapid recovery to very severe and sustained warming in models with a reduced biological adaptation capacity. This tendency for severe warming is caused by a particularly strong reduction in the carbon burial capacity after the LIP-triggered vegetation disturbance (fig. S5) and by the low initial CO_2 concentration that results in a sensitive temperature to CO_2 response (fig. S6), amplifying the warming and vegetation disturbance.

Biogeographic climate sensitivity

Eco-evolutionary dynamics and climate evolution reveal strong interactions with the paleogeographic setting and LIP characteristics. Each geography is characterized by a distinct set of possible climate trajectories after a carbon injection (Fig. 2 and fig. S3). Differences include the tendency for severe and persistent hyperthermals (e.g., Permian-Triassic and present-day configuration) or the chance to result in a warmer climatic quasi–steady state (e.g., Paleocene-Eocene). Our results suggest that these differences are caused by interacting biotic and abiotic factors. Abiotic and geographic factors include the magnitude of the LIP degassing event, the pre-event climate state (i.e., radiative forcing), and the response of temperature and the hydrological cycle to an increase in greenhouse gases (fig. S6). Together, these factors determine the severity of the initial climatic and biological perturbation. The recovery from this perturbation, however, is shaped by interacting biological and abiotic processes, because different geographic configurations cause different local environmental changes and stresses to the vegetation but also shape recovery dynamics by determining possible migration routes. More fragmented continental configurations, such as during the Paleocene-Eocene compared with supercontinent configurations, enhance the likelihood of a shift to a new climatic quasi–steady state because dispersal barriers slow down biological recovery. Differences in the abundance and disturbance of regions with high rates of weathering and primary productivity tend to determine the efficiency of the post-LIP carbon regulation system and the resulting climatic evolution (figs. S5 and S7). The coupled biotic and abiotic response to a perturbation can be considered a biogeographic climate sensitivity that is specific to every paleogeographic configuration and biota present in a given period.

Vegetation eco-evolution and the long-term carbon-climate system

By combining simulations and proxy-based climate reconstructions, we show how the evolution of the physical environment after a LIP-triggered perturbation is shaped by biological vegetation dynamics. Eco-evolutionary processes, including dispersal, evolution, and competition, which determine the resilience and distribution of primary productivity and vegetation-weathering interactions, can interfere with the carbon-climate regulation system, resulting in a large range of possible climate trajectories after a carbon-cycle perturbation. The feedback documented here represents an important addition to the regulation mechanisms previously considered to shape the multimillion-year climate evolution after a massive carbon injection to Earth's atmosphere and oceans (*3*, *35*–*39*).

LIP characteristics, paleogeography, and eco-evolutionary vegetation dynamics combine to shape the temperature trajectories observed in simulations and the data for selected Phanerozoic LIPs. For the Permian-Triassic transition, we observed that the combination of the severe initial warming caused by the Siberian Traps and a limited vegetation adaptation capacity may have reduced the efficiency of the carbon regulation system and resulted in elevated atmospheric CO_2 and temperatures for several million years after the perturbation. Our temperature reconstruction and simulated scenarios are in agreement with other climatic reconstructions for the period (*21*, *22*) and with the especially slow vegetation recovery observed in the fossil record compared with other extinction events (*7*, *15*, *40*, *41*). After the Permian-Triassic mass extinction, it may have taken 4 to 5 Ma for stable forest ecosystems to reestablish (*15*, *42*, *43*). This could have played a particularly large role in slowing down the climatic recovery considering the importance of deep-rooting trees in mediating plant-weathering interactions and carbon assimilation (*13*). By contrast, the geologic record and simulations indicate a faster recovery of temperatures for the Triassic-Jurassic hyperthermal, suggesting that the biogeographic conditions permitted a faster equilibration and recovery of vegetation and the carbon-climate system. Other abiotic and biotic factors could have amplified differences in the vegetation response and climate evolution between the considered LIPs. Short-term "kill mechanisms," such as acid rain, aerosol-induced climatic change, halogen toxicity, and increased levels of ultraviolet B radiation, could have reduced initial vegetation fitness and the ability of vegetation to respond to long-term climate changes (*1*, *44*, *45*). More severe climate warming is further modeled when floras are less adapted at the onset of the LIP, for example, due to a previous climatic perturbation (fig. S9). Distinct environmental perturbations during the LIP emplacement result in different post-LIP plant community structures, with differences in functioning and ecological stability beyond the generalized vegetation response captured in the present model (*40*, *42*, *43*). Additional vegetation adaptation lags could be caused by a limited dispersal success, which is affected not only by the distribution of climatic zones but also by the distribution and formation of appropriate soil conditions (*42*, *46*) and the effect of climatic changes on dispersal vectors (*47*). Our results emphasize the importance of considering such LIP-triggered biological dynamics in shaping the Earth system's response to severe warming.

The LIP-triggered vegetation response can cause a transition to a new climatic quasi–steady state. Combined simulations and data indicate that a new equilibrium can be reached after a multimillion-year high-temperature period (i.e., Permian-Triassic) or relatively rapidly after the initial carbon cycle perturbation, as observed for the Paleocene-Eocene transition. In contrast to the Siberian Traps, the floral recovery after the North Atlantic Igneous Province and the PETM is assumed to have occurred more rapidly through plant dispersal (*48*) and thus less severely affected plant communities (*49*). Our results indicate that for variable speeds of the biological and climatic recovery, a main effect of LIPs is to trigger a process of vegetation turnover and reorganization that can change the long-term rates of organic and inorganic carbon burial. These changes in carbon fluxes result in a new carbon-cycle balance at a different atmospheric CO_2 level than before the perturbation (*50*, *51*). Our findings are supported by limited climatic niche adaptation rates in plants, which are considerably lower than the warming rates during these events (*19*, *20*). Therefore, severe climate changes inevitably result in range shifts, competition, and possibly the extinction of specific floras, which permanently alter the distribution and intensity of vegetation-mediated carbon fluxes. The vegetation reorganization may affect additional vegetation-climate interactions, which can contribute to a shift in the climate state. These include changes in surface albedo, affecting climate through an altered radiation balance [fig. S8; (*52*)], or changes in evapotranspiration rates and water cycling, which may further amplify the influence of vegetation shifts on weathering rates (fig. S3). Biological movement and vegetation dynamics are further shaped by the paleogeographic configuration, which affects the speed of biotic recovery

and therefore the potential for long-term climatic shifts.

Throughout its history, Earth has experienced several severe mass extinctions and finds itself today in another major bioclimatic crisis, this time not triggered by a LIP, but rather by anthropogenic greenhouse gas emissions and land use. Our results show how the coupled response of biological systems and the abiotic environment shape the long-term consequences of such perturbations and reveal the possibility of a shift to a new climatic steady state.

REFERENCES AND NOTES

1. D. P. Bond, P. B. Wignall, in *Volcanism, Impacts, and Mass Extinctions: Causes and Effects*, G. Keller, A. C. Kerr, Eds. (Geological Society of America, 2014), vol. 505; https://doi.org/10.1130/2014.2505(02).
2. M. J. Benton, *Philos. Trans. A Math. Phys. Eng. Sci.* **376**, 20170076 (2018).
3. L. R. Kump, *Philos. Trans. A Math. Phys. Eng. Sci.* **376**, 20170078 (2018).
4. M. T. Jones, D. A. Jerram, H. H. Svensen, C. Grove, *Palaeogeogr. Palaeoclimatol. Palaeoecol.* **441**, 4–21 (2016).
5. J. L. Payne *et al*., *Science* **305**, 506–509 (2004).
6. Z.-Q. Chen, M. J. Benton, *Nat. Geosci.* **5**, 375–383 (2012).
7. Z. Xu *et al*., *Earth Sci. Rev.* **232**, 104136 (2022).
8. P. Hull, *Curr. Biol.* **25**, R941–R952 (2015).
9. L. L. Taylor *et al*., *Geobiology* **7**, 171–191 (2009).
10. K. L. Moulton, *Am. J. Sci.* **300**, 539–570 (2000).
11. J. Quirk, M. Y. Andrews, J. R. Leake, S. A. Banwart, D. J. Beerling, *Biol. Lett.* **10**, 20140375 (2014).
12. E. Berner, R. Berner, K. Moulton, *Treatise on Geochemistry* **5**, 169–188 (2003).
13. J. Quirk *et al*., *Proc. Biol. Sci.* **282**, 20151115 (2015).
14. T. M. Lenton, M. Crouch, M. Johnson, N. Pires, L. Dolan, *Nat. Geosci.* **5**, 86–89 (2012).
15. L. Grauvogel-Stamm, S. R. Ash, *C. R. Palevol* **4**, 593–608 (2005).
16. G. J. Retallack, J. J. Veevers, R. Morante, *Geol. Soc. Am. Bull.* **108**, 195–207 (1999).
17. P. McAllister Rees, *Geology* **30**, 827 (2002).
18. R. T. Corlett, D. A. Westcott, *Trends Ecol. Evol.* **28**, 482–488 (2013).
19. H. Liu, Q. Ye, J. J. Wiens, *Nat. Ecol. Evol.* **4**, 753–763 (2020).
20. J. M. Bennett *et al*., *Nat. Commun.* **12**, 1198 (2021).
21. M. M. Joachimski *et al*., *Geology* **50**, 650–654 (2022).
22. Y. Sun *et al*., *Science* **338**, 366–370 (2012).
23. S. M. Jones, M. Hoggett, S. E. Greene, T. Dunkley Jones, *Nat. Commun.* **10**, 5547 (2019).
24. F. A. McInerney, S. L. Wing, *Annu. Rev. Earth Planet. Sci.* **39**, 489–516 (2011).
25. T. M. Lenton, S. J. Daines, B. J. Mills, *Earth Sci. Rev.* **178**, 1–28 (2018).
26. T. Jezkova, J. J. Wiens, *Proc. Biol. Sci.* **283**, 20162104 (2016).
27. Z. Lososová *et al*., *Glob. Ecol. Biogeogr.* **32**, 1485–1494 (2023).
28. S. V. Sobolev *et al*., *Nature* **477**, 312–316 (2011).
29. H. Svensen *et al*., *Earth Planet. Sci. Lett.* **277**, 490–500 (2009).
30. M. Capriolo *et al*., *Nat. Commun.* **11**, 1670 (2020).
31. M. Steinthorsdottir, A. J. Jeram, J. C. McElwain, *Palaeogeogr. Palaeoclimatol. Palaeoecol.* **308**, 418–432 (2011).
32. C. J. Hollis *et al*., *Geosci. Model Dev.* **12**, 3149–3206 (2019).
33. M. Gutjahr *et al*., *Nature* **548**, 573–577 (2017).
34. M. Storey, R. A. Duncan, C. C. Swisher III, *Science* **316**, 587–589 (2007).
35. T. S. Tobin, C. M. Bitz, D. Archer, *Palaeogeogr. Palaeoclimatol. Palaeoecol.* **478**, 139–148 (2017).
36. R. A. Berner, *Proc. Natl. Acad. Sci. U.S.A.* **99**, 4172–4177 (2002).
37. A. Grard, L. Francois, C. Dessert, B. Dupre, Y. Godderis, *Earth Planet. Sci. Lett.* **234**, 207–221 (2005).
38. Y. Cui, L. R. Kump, *Earth Sci. Rev.* **149**, 5–22 (2015).
39. M. Capriolo *et al*., *Global Planet. Change* **209**, 103731 (2022).
40. J. C. McElwain, S. W. Punyasena, *Trends Ecol. Evol.* **22**, 548–557 (2007).
41. D. H. Erwin, *Proc. Natl. Acad. Sci. U.S.A.* **98**, 5399–5403 (2001).
42. C. V. Looy, W. A. Brugman, D. L. Dilcher, H. Visscher, *Proc. Natl. Acad. Sci. U.S.A.* **96**, 13857–13862 (1999).
43. C. V. Looy, R. J. Twitchett, D. L. Dilcher, J. H. A. Van Konijnenburg-Van Cittert, H. Visscher, *Proc. Natl. Acad. Sci. U.S.A.* **98**, 7879–7883 (2001).
44. B. A. Black, L. T. Elkins-Tanton, M. C. Rowe, I. U. Peate, *Earth Planet. Sci. Lett.* **317-318**, 363–373 (2012).
45. B. A. Black *et al*., *Nat. Geosci.* **11**, 949–954 (2018).
46. M. A. Sephton *et al*., *Geology* **33**, 941 (2005).
47. J. C. McElwain, M. E. Popa, S. P. Hesselbo, M. Haworth, F. Surlyk, *Paleobiology* **33**, 547–573 (2007).
48. S. L. Wing *et al*., *Science* **310**, 993–996 (2005).
49. C. Jaramillo *et al*., *Science* **330**, 957–961 (2010).
50. M. P. D'Antonio, D. E. Ibarra, C. K. Boyce, *Geology* **48**, 29–33 (2020).
51. B. J. W. Mills, S. Tennenbaum, D. Schwartzman, *Am. J. Sci.* **321**, 1033–1044 (2021).
52. Y. Donnadieu, Y. Godderis, N. Bouttes, *Clim. Past* **5**, 85–96 (2009).
53. Proxy data for the paleotemperature estimations for: J. Rogger *et al*., Biogeographic climate sensitivity controls earth system response to large igneous province carbon degassing, Zenodo (2022); https://doi.org/10.5281/zenodo.7275402.
54. E. J. Judd *et al*., *Sci. Data* **9**, 753 (2022).
55. Model and analysis code for: J. Rogger *et al*., Biogeographic climate sensitivity controls Earth system response to large igneous province carbon degassing, Zenodo (2024); https://doi.org/10.5281/zenodo.12187757.
56. C. Scotese, N. Wright, "PALEOMAP Paleodigital Elevation Models (PaleoDEMS) for the Phanerozoic." Available from: https://www.earthbyte.org/paleodem-resource-scotese-and-wright-2018/ (2018).
57. E. O. Straume, C. Gaina, K. H. Nisancioglu, *Gondwana Res.* **86**, 126–143 (2020).

ACKNOWLEDGMENTS

We thank M. Dawes for English editing. All model simulations were conducted on the ETH Zurich computer cluster "Euler." **Funding:** This work was supported by the Swiss National Science Foundation ("Biogeodynamics" grant 192296 to J.R., T.V.G., and L.P.) and UK Research and Innovation (projects EP/Y008790/1 and NE/X011208/1 to B.J.W.M.). **Author contributions:** Conceptualization: J.R., E.J.J., B.J.W.M., Y.G., T.V.G., L.P.; Formal analysis: J.R., E.J.J.; Funding acquisition: T.V.G., L.P.; Investigation: J.R., E.J.J.; Methodology: J.R., E.J.J., B.J.W.M., Y.G., T.V.G., L.P.; Software: J.R.; Supervision: T.V.G., L.P.; Validation: J.R., E.J.J., B.J.W.M., Y.G., T.V.G., L.P.; Visualization: J.R., E.J.J.; Writing – original draft: J.R., E.J.J., B.J.W.M., Y.G., T.V.G., L.P.; Writing – review & editing: J.R., E.J.J., B.J.W.M., Y.G., T.V.G., L.P. **Competing interests:** The authors declare no competing interests. **Data and materials availability:** All data sources are available in the main manuscript or the supplementary materials. Proxy data for the paleotemperature estimations are available at Zenodo (*53*), with further details described in (*54*). Model and analysis code are available at Zenodo (*55*). **License information:**

SUPPLEMENTARY MATERIALS

science.org/doi/10.1126/science.adn3450
Materials and Methods
Figs. S1 to S13
References (*58–87*)
MDAR Reproducibility Checklist

Submitted 5 December 2023; accepted 5 July 2024
10.1126/science.adn3450